UC Berkeley
UC Berkeley Previously Published Works

Title
Reticular Growth of Graphene Nanoribbon 2D Covalent Organic Frameworks

Permalink
https://escholarship.org/uc/item/5f25h6wn

Journal
Chem, 6(5)

Authors

Veber, Gregory
Diercks, Christian S
Rogers, Cameron
et al.

Publication Date
2020-05-01

Peer reviewed

Chem

Article

Reticular Growth of Graphene Nanoribbon 2D Covalent Organic Frameworks

Bottom-Up Synthesis of Graphene Nanoribbons (GNRs)

Interfacial Growth of GNR-COFs

Liquid Phase Exfoliation of GNR-COFs
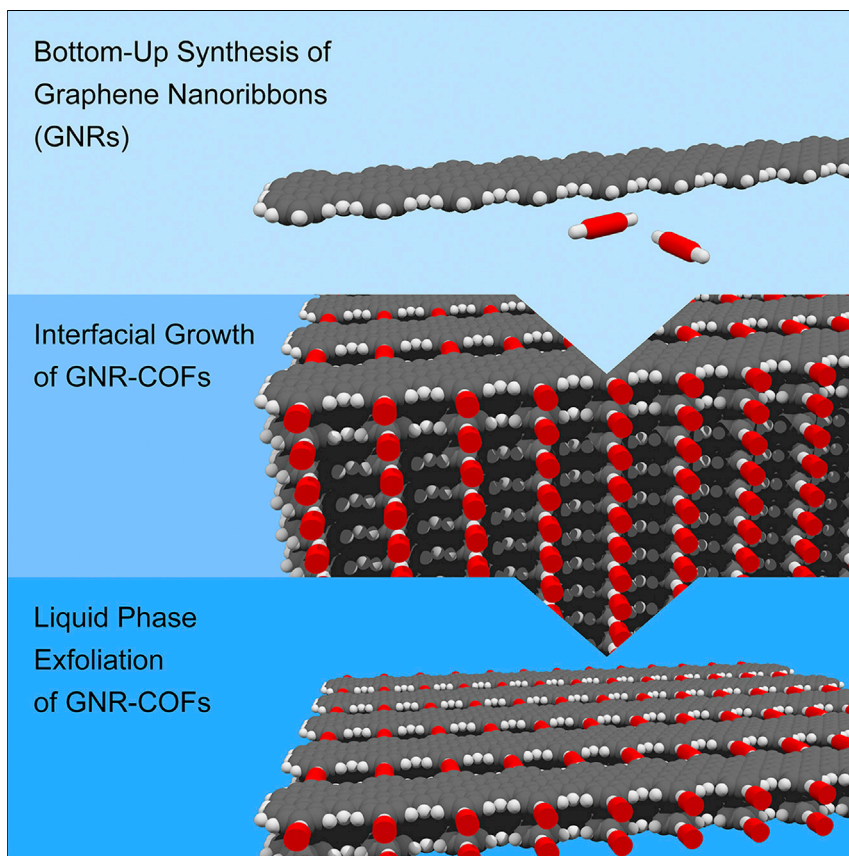
Fischer and co-workers present the realization of a porous crystalline two dimensional (2D) covalent organic framework (COF) grown from a polydisperse macromolecular building block. Bottom-up synthesized graphene nanoribbons (GNRs), quasi-one-dimensional (1D) atomically defined strips of single-layer graphene, self-assemble at a liquid-liquid interface into π-stacked 2D sheets cross-linked by diamine spacers. This distinct class of infinitely tunable 2D layered materials is anticipated to give rise to correlated phenomena emerging from the intrinsic anisotropy of constituent 1D GNR building blocks.

Gregory Veber, Christian S. Diercks, Cameron Rogers, ..., Chenhui Zhu, Jeffrey Bokor, Felix R. Fischer

ffischer@berkeley.edu

HIGHLIGHTS

A crystalline COF was grown from polydisperse 1D graphene nanoribbons (GNRs)

XRD reveals the intrinsic anisotropy of the 2D COF grown at a liquid-liquid interface

Crystalline domains of parallel GNRs enhance the bulk conductance in COF thin films

Multilayer 2D GNR-COF sheets can be delaminated to give access to few-layer GNR-COFs

Article

Reticular Growth of Graphene Nanoribbon 2D Covalent Organic Frameworks

Gregory Veber,[1] Christian S. Diercks,[1] Cameron Rogers,[1] Wade S. Perkins,[1] Jim Ciston,[2] Kyunghoon Lee,[3] Juan Pablo Llinas,[3] Alex Liebman-Peláez,[4] Chenhui Zhu,[4] Jeffrey Bokor,[3,5] and Felix R. Fischer[1,5,6,7,*]

SUMMARY

The reticular synthesis of covalent organic frameworks (COFs), extended porous two-dimensional (2D) or three-dimensional (3D) networks held together by strong, highly directional chemical bonds, has thus far been restricted to small, shape-persistent, molecular building blocks. Here, we demonstrate the growth of crystalline 2D COFs from a polydisperse macromolecule derived from single-layer graphene, bottom-up synthesized quasi-one-dimensional (1D) graphene nanoribbons (GNRs). X-ray scattering and transmission electron microscopy reveal that 2D sheets of GNR-COFs self-assembled at a liquid-liquid interface stack parallel to the layer boundary and exhibit an orthotropic crystal packing. Liquid-phase exfoliation of multilayer GNR-COF crystals gives access to large-area ($>10^5$ nm^2) bilayer and trilayer cGNR-COF films. The functional integration of extended 1D materials into crystalline COFs greatly expands the structural complexity and the scope of mechanical and physical materials properties accessible through a deterministic reticular bottom-up approach.

INTRODUCTION

Covalent organic frameworks (COFs) are 2D or 3D extended periodic networks assembled from symmetric, shape-persistent molecular building blocks through strong, directional bonds.[1,2] Traditional COF growth strategies heavily rely on reversible condensation reactions that guide the reticulation toward a desired thermodynamic equilibrium structure.[3] The requirement for dynamic error correction, however, limits the choice of building blocks and thus the associated mechanical and electronic properties imbued within the periodic lattice of the COF. Furthermore, the poor electronic communication across imine and boronate ester linkers, most commonly used in the synthesis of 2D COFs, gives rise to semiconducting materials featuring large band gaps undesirable for advanced electronic applications.[4,5] Charge-carrier transport in these materials is dominated by interlayer hopping mechanisms rather than through chemical bonds between linkers and the constituent molecular building blocks within a 2D sheet.[6] Introduction of conjugated polymers as 1D conduction paths within a single COF sheet could address this shortcoming, yet the incorporation of macromolecules as building units in COFs has not been demonstrated. Recent advances in the bottom-up synthesis of graphene nanoribbons (GNRs), atomically thin quasi-1D strips of graphene, have inspired the development of a unique class of COF building blocks. The control over key structural parameters in GNRs, width,[7–10] edge symmetry,[7,11,12] dopant atom density,[13–15] and dopant position[16,17] gives rise to a highly tunable band structure and the emergence of exotic physical phenomena linked to symmetry protected topological states.[18,19]

The Bigger Picture

Covalent organic frameworks (COFs) are a promising class of 2D materials for a variety of applications ranging from molecular sieves to organic electronics. Thus far the formation of these materials has been limited to discrete small molecule precursors utilized to reticulate the 2D or 3D networks. Here, we demonstrate the synthesis of a crystalline COF network derived from conductive 1D nanowires known as graphene nanoribbons (GNRs). Furthermore, we show that bilayer and trilayer GNR-COF films can be obtained via a liquid-phase exfoliation protocol. Now the chemical library for COF precursors has been expanded to include macromolecules and even carbon nanomaterials thus opening the opportunity to explore interesting materials properties emerging from polymer reticulation such as anisotropic charge transport and non-linear optoelectronic properties.

Here, we show that the exquisite structural control inherent to bottom-up synthesized GNRs can be adapted to introduce atomically precise spacings of functional groups along the edges of a ribbon, giving access to a shape-persistent quasi-1D macromolecular building block for the reticular synthesis of 2D COFs.

Imine linked GNR-COF films were assembled from aldehyde functionalized cove-GNRs (CHO-cGNR) and benzidine crosslinkers. Large area, homogeneous thin films of variable thickness were synthesized through interfacial polymerization at a liquid-liquid interface. By modulating the concentration of GNRs in the reaction mixture the film thickness can be controlled over a range of 2–22 nm. Fourier transform infrared (FT-IR) spectroscopy along with control experiments using unfunctionalized cGNRs confirmed that the GNR-COF films are covalently linked through imine bonds. The crystallographic structure of the GNR-COF was probed by using wide-angle X-ray scattering (WAXS) and transmission electron microscopy (TEM), revealing the extraordinary potential of reticular covalent self-assembly techniques to access densely packed parallel arrays of GNRs. Liquid-phase exfoliation of crystalline cGNR-COFs gives access to vertically stacked few-layered cGNR-COF flakes for applications in functional materials and advanced electronics.

RESULTS AND DISCUSSION

Synthesis and Characterization of CHO-cGNR

The synthesis of CHO-cGNRs is depicted in Figure 1A. Diels-Alder polymerization of acetal protected cyclopentadienone **3** yields the poly-phenylene precursor **4**. Size exclusion chromatography (SEC) shows a bimodal distribution of linear polymers (M_n = 26,000 g mol^{-1}) and cyclic oligomers (M_n = 3,000 g mol^{-1}) (Figure S1) characteristic for a step-growth polymerization mechanism.[20,21] Acid catalyzed deprotection of crude **4** yields the aldehyde functionalized poly-phenylene **5**. Fractionation of the polymer mixture by preparative SEC gave access to samples of high molecular weight linear polymer **5** (M_n = 18,500 g mol^{-1}) and low molecular weight cyclic oligomers (M_n = 2,100 g mol^{-1}) (Figure 1B). MALDI mass spectroscopy of linear polymers **4** and **5** shows families of molecular ions separated by the repeat unit of the polymers, 676 g mol^{-1} and 588 g mol^{-1} for **4** and **5**, respectively (Figure 1C). The successful deprotection of **4** is further corroborated by the absence of characteristic peaks associated with the acetal protecting group (δ = 4.16–3.89 ppm) in ^{1}H-NMR spectra of **5** and the appearance of a new peak consistent with the aldehyde group hydrogen atoms (δ = 10.06–9.85 ppm) (Figure S2). Oxidative cyclodehydrogenation of **5** yields CHO-cGNR as a dark solid. Raman spectra of CHO-cGNRs show the characteristic signatures of cGNRs; a radial breathing like mode (RBLM) (253 cm^{-1}), the D (1,332 cm^{-1}), and the G (1,603 cm^{-1}) peaks as well as overtone 2D, D+D′, and 2D′ peaks (Figures 1D and S3).[20,22,23] An overlay of the respective IR spectra of poly-phenylene **5** and CHO-cGNR confirms the presence of aldehyde groups in the GNRs. The relative intensity of the characteristic aldehyde C=O stretching mode at 1,699 cm^{-1}, with respect to the C=C stretching mode at 1,602 cm^{-1}, remains unchanged after the oxidative cyclodehydrogenation (Figure 1E). The UV-vis absorption spectrum of aldehyde functionalized CHO-cGNRs, indistinguishable from an original sample of cGNRs featuring solubilizing alkyl chains (Figure S4),[23] along with the characteristic Raman spectra (Figure 1D), is further evidence that the oxidative cyclodehydrogenation proceeds to the expected high degree of conversion.[20,23]

Interfacial 2D cGNR-COF Growth

Imine cross-linked crystalline cGNR-COFs were grown by using a Lewis acid catalyzed interfacial polymerization.[24–26] The physical separation of the catalyst (Sc(OTf)$_3$), dissolved in an aqueous phase, and the organic building blocks, CHO-cGNRs and the benzidine cross-linker dispersed in an immiscible organic phase,

[1]Department of Chemistry, University of California Berkeley, Berkeley, CA 94720, USA

[2]National Center for Electron Microscopy, Molecular Foundry, Lawrence Berkeley National Laboratory, Berkeley, CA 94720, USA

[3]Department of Electrical Engineering and Computer Sciences, University of California Berkeley, Berkeley, CA 94720, USA
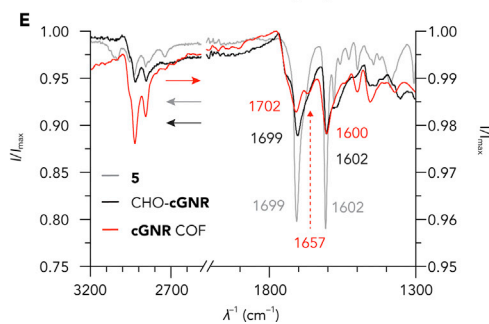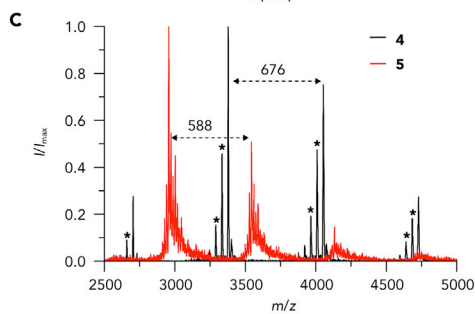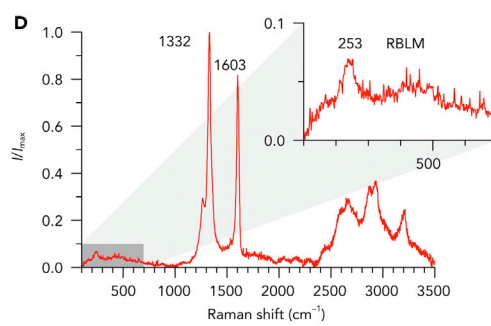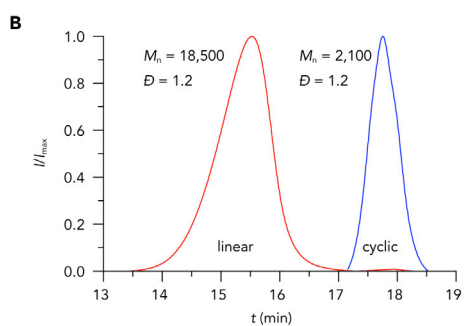
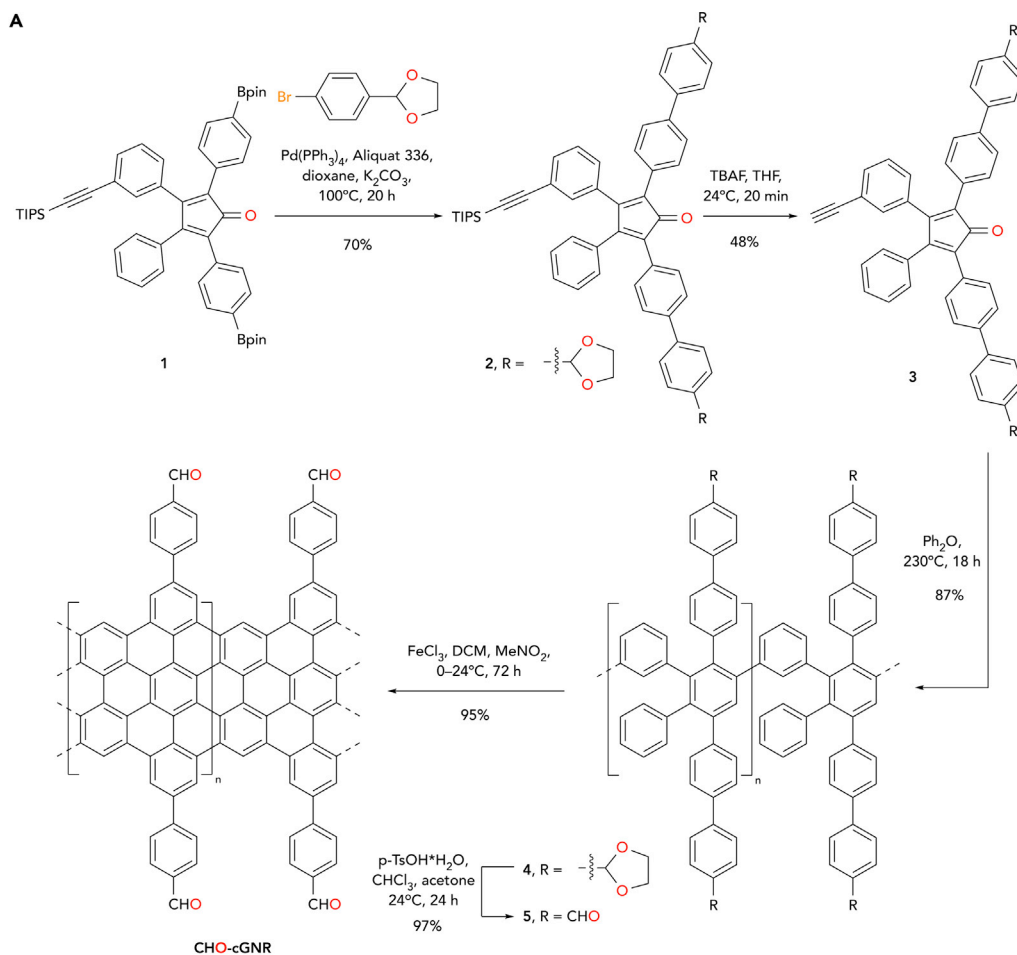[4]Advanced Light Source, Lawrence Berkeley National Laboratory, Berkeley, CA 94720, USA

[5]Materials Sciences Division, Lawrence Berkeley National Laboratory, Berkeley, CA 94720, USA

[6]Kavli Energy NanoSciences Institute at the University of California Berkeley and the Lawrence Berkeley National Laboratory, Berkeley, CA 94720, USA

[7]Lead Contact

*Correspondence: ffischer@berkeley.edu

A

1 → 2, R = (1,3-dioxolane)
2 → 3

Pd(PPh₃)₄, Aliquat 336, dioxane, K₂CO₃, 100°C, 20 h — 70%

TBAF, THF, 24°C, 20 min — 48%

Ph₂O, 230°C, 18 h — 87%

FeCl₃, DCM, MeNO₂, 0–24°C, 72 h — 95%

p-TsOH*H₂O, CHCl₃, acetone 24°C, 24 h — 97%

4, R = (1,3-dioxolane)
5, R = CHO

CHO-cGNR

B

$M_n = 18{,}500$, $Đ = 1.2$ (linear)
$M_n = 2{,}100$, $Đ = 1.2$ (cyclic)

C

— 4
— 5

588, 676

D

1332, 1603
253 RBLM

E

— **5**
— CHO-**cGNR**
— **cGNR** COF

1702, 1699, 1657, 1600, 1602, 1699, 1602

Figure 1. Synthesis and Characterization of Aldehyde Functionalized CHO-cGNRs

(A) Schematic representation of the synthesis of CHO-cGNR.

(B) SEC traces for the linear polymers (red) and cyclic oligomers (blue) of **5**.

(C) MALDI mass spectrum of crude **4** (black) and **5** (red) showing families of molecular ions separated by the mass of each polymer repeat unit (* corresponds to subfamilies of molecular ions resulting from the loss of acetal protecting groups).

(D) Raman spectrum (λ_E = 532 nm) of CHO-cGNRs. Inset shows the characteristic RLBM of cGNRs. See also Figure S3.

(E) FT-IR spectrum of **5** (gray), CHO-cGNRs (black), and cGNR-COF (red) showing the characteristic aldehyde C=O (λ^{-1} = 1,699 cm^{-1}) and aromatic C=C (λ^{-1} = 1,602 cm^{-1}) stretching modes in both **5** and CHO-cGNRs. The IR spectrum of cGNR-COF shows a decrease in the intensity of the aldehyde C=O (λ^{-1} = 1,702 cm^{-1}) relative to the C=C mode (λ^{-1} = 1,600 cm^{-1}) along with the signal for the C=N imine stretching mode (λ^{-1} = 1,657 cm^{-1}). See also Figure S7.

relegate the COF film growth exclusively to the liquid-liquid interface. The limited stability of dispersions of CHO-cGNRs in a wide variety of solvents along with the requirement that the density of the organic phase be greater than the aqueous phase to prevent the undesired precipitation of amorphous GNR aggregates at the liquid-liquid interface during film growth, narrowed the selection of organic solvents to mixtures of o-dichlorobenzene (o-DCB) and chloroform. High quality cGNR-COFs were obtained by layering an aqueous solution of Sc(OTf)$_3$ (5 mM) over a homogeneous dispersion of CHO-cGNRs and benzidine in o-DCB/CHCl$_3$ (v/v = 1:1). Over the course of 5–7 days gray films form at the liquid-liquid boundary that were scooped from the interface and transferred onto solid substrates (Figure 2A). A series of control experiments that alternately remove any one of the critical components, CHO-cGNRs, benzidine cross-linker, or Sc(OTf)$_3$, from the reaction mixture preclude the formation of cGNR-COFs even after extended reaction times. Similarly, the replacement of CHO-cGNRs with unfunctionalized cGNRs did not lead to the formation of COF films at the liquid-liquid interface (Figure S5). We, therefore, conclude that the observed cGNR-COF films formed in the presence of both reaction partners, CHO-cGNRs, benzidine, and the Lewis acid catalyst are not comprised of non-covalently assembled films formed at the interface solely driven by π-π interactions.

Optical microscopy of cGNR-COFs transferred onto a Si/SiO$_2$ surface reveal large flakes (>1,000 μm^2) of uniform color contrast (Figure 2B). Raman spectra recorded at various positions on cGNR-COF films show the characteristic RBLM, D, and G peaks associated with CHO-cGNRs, supporting the structural assignment (Figure 2C, blue and red traces). Areas of the SiO$_2$ apparently devoid of cGNR-COFs show only very weak Raman signatures (Figure 2C, black trace), attributed to small GNR aggregates or individual ribbons transferred with the solvent during the scooping process. Spatial Raman maps of the G-peak intensity of cGNR-COFs on Si/SiO$_2$ seamlessly coincide with the optical contrast in microscopy images (Figure S6). Attenuation of the FT-IR spectra recorded on transferred cGNR-COFs reveal the formation of imine bonds within the film. The FT-IR spectrum of the cGNR-COF, as compared with the CHO-cGNR, shows a decrease in the intensity of the characteristic aldehyde C=O stretching mode (λ^{-1} = 1,702 cm^{-1}) relative to the C=C mode (λ^{-1} = 1,600 cm^{-1}) (Figures 1E and S7). The imine C=N stretching mode resulting from the crosslinking of CHO-cGNRs with benzidine appears as a new shoulder at λ^{-1} = 1,657 cm^{-1} in the IR spectrum of cGNR-COFs (Figures 1E and S7).

cGNR-COF film morphology and thickness were examined by using scanning electron microscopy (SEM) and atomic force microscopy (AFM). SEM images of cGNR-COF films transferred onto TEM grids show large-scale homogeneity and well-defined film morphology (Figure 2D). Large areas (>100 μm^2) of homogeneous, smooth films show little to no amorphous regions or protrusions from the surface (Figure 2D). This is further supported by ambient AFM that shows films with height profiles ranging from 2–20 nm (Figures 2E and S8). The thickness of cGNR-COF films
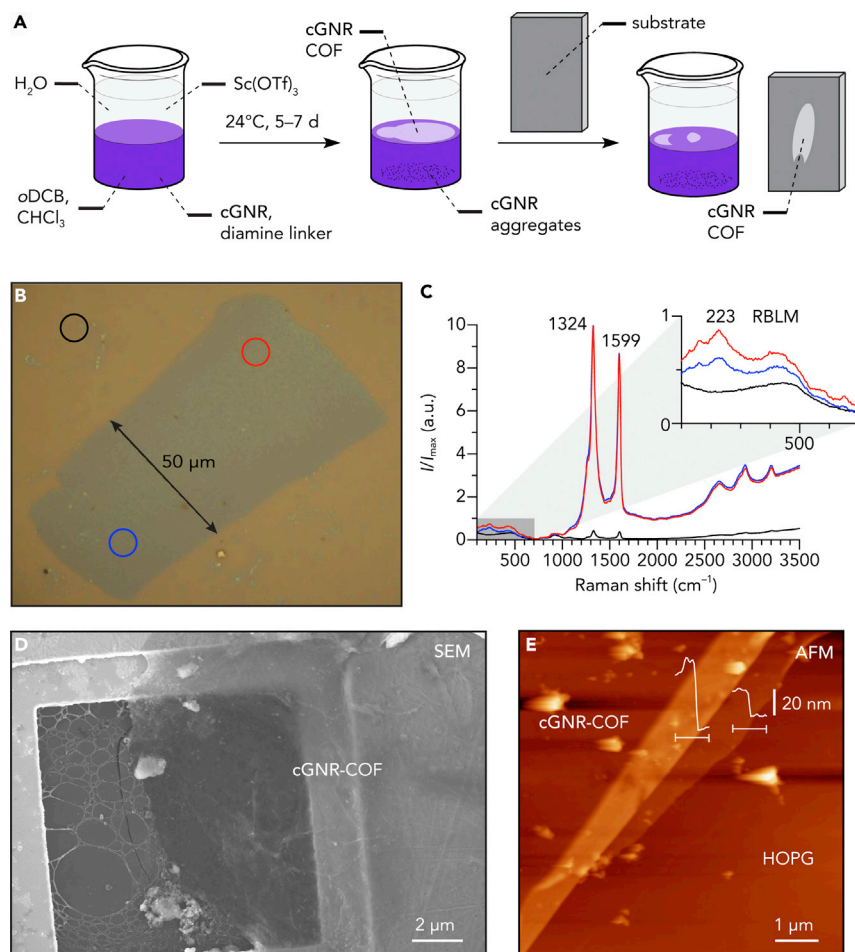
Figure 2. Synthesis and Characterization of cGNR-COF Thin Films

(A) Schematic representation of the interfacial polymerization and scooping transfer process.

(B) Optical microscopy image of a transferred cGNR-COF film on Si/SiO_2. Circles correspond to positions where Raman spectra were recorded. See also Figure S5.

(C) Raman spectra (λ_E = 532 nm) of the three regions highlighted in (B). Inset shows the characteristic RBLM. See also Figure S6.

(D) Scanning electron microscope image of cGNR-COF film dispersion dropcast onto a TEM grid (5 kV accelerating voltage).

(E) Atomic force microscopy (AFM) of ~20 nm cGNR-COF film on HOPG. Film thickness in folded regions corresponds to integer multiples of the single-layer film (~40 nm). See also Figure S8.

prepared through Lewis acid catalyzed growth at the liquid-liquid interface scales linearly with the initial concentration of CHO-cGNRs (Figure S9). Dilute dispersions of CHO-cGNRs (67 μg mL^{-1}) yield film thicknesses as low as 2 nm, whereas higher concentrations (270 μg mL^{-1}) form films with average thicknesses in excess of 20 nm.

We used synchrotron X-ray scattering to study the crystallographic structure of cGNR-COFs films. Figure 3A shows the projected trace of the wide-angle X-ray scattering (WAXS) pattern of powdered samples of cGNR-COFs grown at the liquid-liquid interface. The data were collected by suspending a dried, powdered sample of cGNR-COFs in a quartz capillary perpendicular to the incident beam. The WAXS pattern shows three characteristic reflections at 2θ = 3.5°, 7.0°, and 12.0° corresponding to d-spacings of 2.5, 1.2, and 0.7 nm, respectively (Figure 3A). A structure model for the packing of cGNR-COF constructed in the triclinic space group P–1 with unit cell parameters
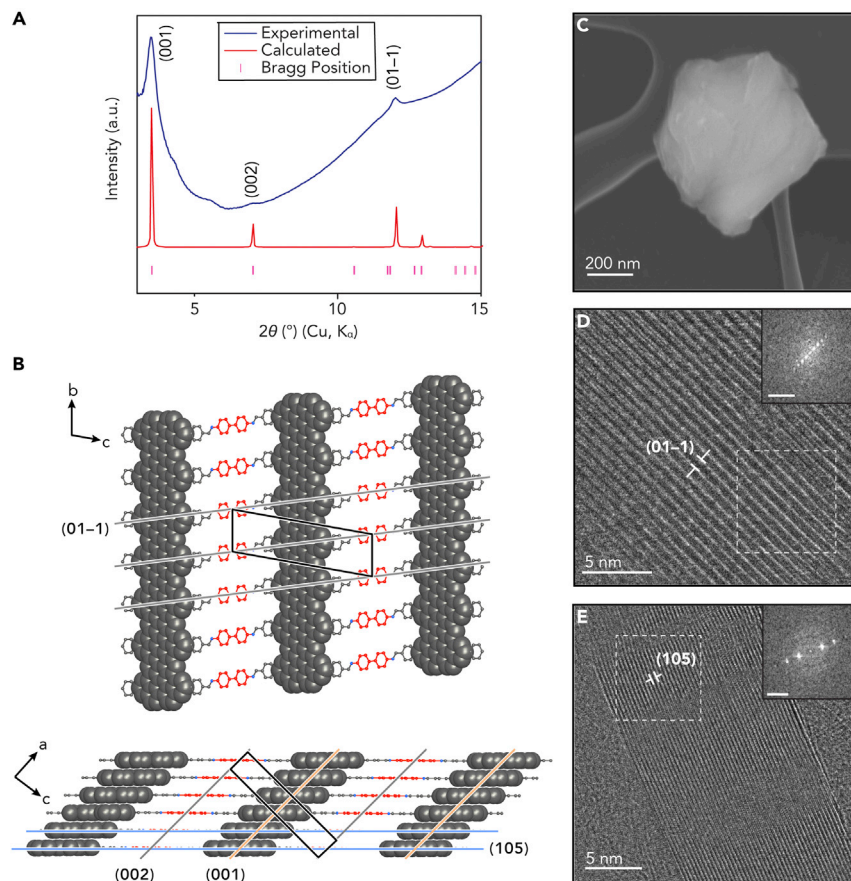
Figure 3. Powder X-ray Diffraction and HR-TEM of cGNR-COF Thin Films

(A) Experimentally and theoretically calculated WAXS pattern of powdered sample of cGNR-COF film.

(B) Structural model of cGNR-COF with unit cell (black box), orientation displaying lattice plane (01−1) corresponding to distance between linkers (0.7 nm) (top), orientation displaying interlayer packing and lattice planes (001) (orange), (002) (gray), and (105) (blue) corresponding to 2.5, 1.25, and 0.35 nm (bottom).

(C) Scanning electron microscope image of cGNR-COF film from HR-TEM sample.

(D) HR-TEM image of cGNR-COF crystallite displaying the (01−1) plane, fringes separated by 0.7 nm (white marker), Fourier diffractogram of the highlighted region (inset; scale bar, 5 nm^{-1}).

(E) HR-TEM image of cGNR-COF crystallite displaying the (105) plane, fringes represent π-π-stacking (0.35 nm) within the film, Fourier diffractogram of the highlighted region (inset; scale bar, 5 nm^{-1}).

a = 5.0 Å, b = 7.4 Å, c = 25.5 Å, α = 100°, β = 90°, and γ = 90° is depicted in Figure 3B (Table S1). The predicted diffraction pattern is in good agreement with experimental data. The observed reflections at 2.5, 1.2, and 0.7 nm were assigned to the (001), (002), and (01−1) planes, respectively (Figure 3A). The (001) and (002) Bragg reflections correspond to the distance, and half the distance, between parallel ribbons (2.5 and 1.25 nm) whereas the (01−1) corresponds to the spacing of benzidine linkers (0.7 nm) lining the edges of the cGNRs (Figure 3B). The Bragg reflection associated with the interlayer π-stacking between cGNRs is masked by the pronounced background of the quartz capillary in the expected region of the WAXS pattern.

We used high-resolution transmission electron microscopy (HR-TEM) to study the crystalline domain size of cGNR-COF films directly scooped from the liquid-liquid

interphase (Figure 3C). The micrographs, recorded at a total electron dose of 100 e Å^{-2} to minimize sample damage, display clear lattice fringes corresponding to the distance between linkers (0.7 nm) (Figure 3D) and the π-stacking between ribbons (0.35 nm) (Figure 3E), respectively. The observed lattice fringes corroborate the molecular model depicted in Figure 3B and can be assigned to the (01–1) and (105) lattice planes, respectively. The fact that the (001) and (002) planes related to the distance between covalently linked cGNRs cannot be observed in the TEM images is attributed to a preferential orientation of the crystallites within the film relative to the TEM grid. After the scooping transfer the cGNR-COFs adopt orientations in which the lateral spacing between cGNRs (2.5 nm) lies on an axis perpendicular to the surface and remains out of focus leaving only the π-stacking and linker-linker distances to be observed by in-plane elastic scattering. Most notably, the HR-TEM demonstrates that the crystalline domain size (>400 nm^2) is 1–2 orders of magnitude larger than previously reported solution processable GNR films formed via π-stacking alone.[27] cGNR-COFs not only self-assemble into larger crystallites but macromolecular reticulation through directional covalent bonds allows for the rational design of highly anisotropic materials.

Electrical Conductance of Multilayered cGNR-COF Films

Next, we explored the electrical conductance within the crystalline domains in cGNR-COF films. Large-area thick (>10 nm) cGNR-COF films were directly scooped from the liquid-liquid interface onto Al_2O_3 substrates prepatterned with Pt electrodes. Figure S10 shows a representative optical microscopy image of a large (>10^4 μm^2) cGNR-COF film bridging the gap between multiple prepatterned electrodes. Even in the absence of a gate bias ($V_g = 0$ V) cGNR-COF devices exhibit drain currents (I_{ds}) as large as 2 nA at very low source-drain bias ($V_{ds} = 10$ V) when compared with dropcast π-stacked GNR thin films.[27] These initial I–V characteristics suggest that the presence of crystalline domains within these multilayered cGNR-COF films contribute to an enhancement of the bulk conductivity across sizable areas of the film.

Liquid-Phase Exfoliation of cGNR-COF Films

Finally, adopting a liquid-phase exfoliation protocol for the delamination of crystalline 2D COFs, we were able to access free-standing few-layer 2D cGNR-COF sheets. A dispersion of multilayer films grown from a saturated CHO-cGNR solution in acetone was transferred to o-DCB, sonicated, and dropcast onto Si/SiO$_2$. The resulting cGNR-COF flakes were analyzed using ambient AFM to determine the film thickness, size, and homogeneity (Figures 4A and 4B). The lateral dimensions of the cGNR-COF flakes are >10^5 nm^2 and range in thickness between 0.70 nm (Figure 4C) and 1.05 nm (Figure 4D), corresponding to bilayer and trilayer stacks of 2D cGNR-COF sheets (π-π-stacking distance $\Delta = 0.35$ nm). Some exfoliated films exhibit layered height profiles commensurate with step-edges within a single flake (Figure S11).

The orthotropic crystal packing adopted by GNRs in 2D COF films represents a unique opportunity to enhance the chemical, physical, and optoelectronic properties of COFs by independently tuning the mechanical and electrical material properties along all three axes of the crystal lattice. The simplicity of our interfacial GNR-COF growth and liquid-phase exfoliation protocol opens the path to accessing densely packed 2D sheets of parallel GNRs for high-performance electronic device architectures and the exploration of exotic physical phenomena emerging from deterministically engineered stacks of anisotropic layered 2D materials.
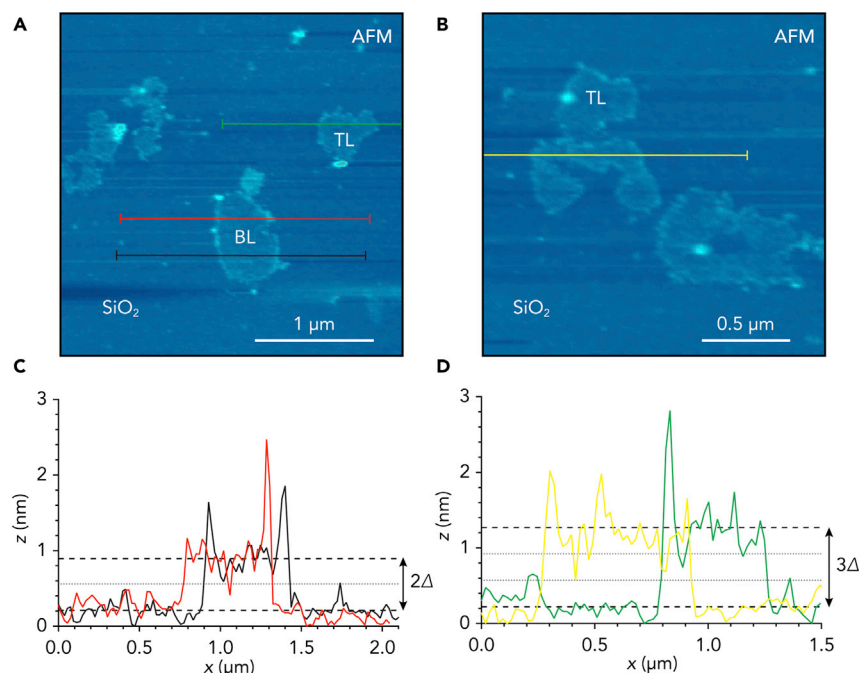
Figure 4. Chemically Exfoliated Bilayer and Trilayer cGNR-COF Flakes on SiO₂ Substrates

(A) AFM topographic images of liquid-phase exfoliated cGNR-COF on SiO$_2$.

(B) AFM topographic images of liquid-phase exfoliated cGNR-COF on SiO$_2$.

(C) AFM z-height profiles along the lines depicted in (A). Averaged background and averaged plateau height (black dashed lines), spacing corresponding to interlayer π-π-stacking distance (Δ = 0.35 nm) as determined via HR-TEM and diffraction models (gray dotted lines). See also Figure S11.

(D) AFM z-height profiles along the lines depicted in (B). Averaged background and averaged plateau height (black dashed lines), spacing corresponding to interlayer π-π-stacking distance (Δ = 0.35 nm) as determined via HR-TEM, and diffraction models (gray dotted lines).

EXPERIMENTAL PROCEDURES

All experimental details are presented in the Supplemental Information.

SUPPLEMENTAL INFORMATION

Supplemental Information can be found online at https://doi.org/10.1016/j.chempr.2020.01.022.

AUTHOR CONTRIBUTIONS

G.V. and F.R.F. conceived the experiments. G.V. performed synthesis, COF growth, sample preparation, characterization, and data analysis. G.V. and C.R. performed

SEM. G.V. and W.S.P. performed ambient AFM. C.Z. and A.L.-P. performed X-ray diffraction. C.S.D. performed diffraction data analysis and modeling. J.C. performed TEM. K.L. and J.P.L. performed electrical conductivity measurements. G.V., C.S.D., and F.R.F contributed to writing of the paper.

DECLARATION OF INTERESTS

The authors declare no competing interests.

REFERENCES

1. Diercks, C.S., and Yaghi, O.M. (2017). The atom, the molecule, and the covalent organic framework. Science 355, 6328.

2. Colson, J.W., and Dichtel, W.R. (2013). Rationally synthesized two-dimensional polymers. Nat. Chem. 5, 453–465.

3. Smith, B.J., Overholts, A.C., Hwang, N., and Dichtel, W.R. (2016). Insight into the crystallization of amorphous imine-linked polymer networks to 2D covalent organic frameworks. Chem. Commun. (Camb.) 52, 3690–3693.

4. Joshi, T., Chen, C., Li, H., Diercks, C.S., Wang, G., Waller, P.J., Li, H., Bredas, J.L., Yaghi, O.M., and Crommie, M.F. (2019). Local electronic structure of molecular heterojunctions in a single-layer 2D covalent organic framework. Adv. Mater. 31, e1805941.

5. Chen, C., Joshi, T., Li, H., Chavez, A.D., Pedramrazi, Z., Liu, P.N., Li, H., Dichtel, W.R., Bredas, J.L., and Crommie, M.F. (2018). Local electronic structure of a single-layer porphyrin-containing covalent organic framework. ACS Nano 12, 385–391.

6. Dogru, M., and Bein, T. (2014). On the road towards electroactive covalent organic frameworks. Chem. Commun. (Camb.) 50, 5531–5546.

7. Cai, J., Ruffieux, P., Jaafar, R., Bieri, M., Braun, T., Blankenburg, S., Muoth, M., Seitsonen, A.P., Saleh, M., Feng, X., et al. (2010). Atomically precise bottom-up fabrication of graphene nanoribbons. Nature 466, 470–473.

8. Chen, Y.C., De Oteyza, D.G., Pedramrazi, Z., Chen, C., Fischer, F.R., and Crommie, M.F. (2013). Tuning the band gap of graphene nanoribbons synthesized from molecular precursors. ACS Nano 7, 6123–6128.

9. Talirz, L., Söde, H., Dumslaff, T., Wang, S., Sanchez-Valencia, J.R., Liu, J., Shinde, P., Pignedoli, C.A., Liang, L., Meunier, V., et al. (2017). On-surface synthesis and characterization of 9-atom wide armchair graphene nanoribbons. ACS Nano 11, 1380–1388.

10. Zhang, H., Lin, H., Sun, K., Chen, L., Zagranyarski, Y., Aghdassi, N., Duhm, S., Li, Q., Zhong, D., Li, Y., et al. (2015). On-surface synthesis of rylene-type graphene nanoribbons. J. Am. Chem. Soc. 137, 4022–4025.

11. Liu, J., Li, B.W., Tan, Y.Z., Giannakopoulos, A., Sanchez-Sanchez, C., Beljonne, D., Ruffieux, P., Fasel, R., Feng, X., and Müllen, K. (2015). Toward cove-edged low band gap graphene nanoribbons. J. Am. Chem. Soc. 137, 6097–6103.

12. Ruffieux, P., Wang, S., Yang, B., Sánchez-Sánchez, C., Liu, J., Dienel, T., Talirz, L., Shinde, P., Pignedoli, C.A., Passerone, D., et al. (2016). On-surface synthesis of graphene nanoribbons with zigzag edge topology. Nature 531, 489–492.

13. Cai, J., Pignedoli, C.A., Talirz, L., Ruffieux, P., Söde, H., Liang, L., Meunier, V., Berger, R., Li, R., Feng, X., et al. (2014). Graphene nanoribbon heterojunctions. Nat. Nanotechnol. 9, 896–900.

14. Bronner, C., Stremlau, S., Gille, M., Brauße, F., Haase, A., Hecht, S., and Tegeder, P. (2013). Aligning the band gap of graphene nanoribbons by monomer doping. Angew. Chem. Int. Ed. Engl. 52, 4422–4425.

15. Zhang, Y., Zhang, Y., Li, G., Lu, J., Lin, X., Du, S., Berger, R., Feng, X., Müllen, K., and Gao, H.J. (2014). Direct visualization of atomically precise nitrogen-doped graphene nanoribbons. Appl. Phys. Lett. 105.

16. Cloke, R.R., Marangoni, T., Nguyen, G.D., Joshi, T., Rizzo, D.J., Bronner, C., Cao, T., Louie, S.G., Crommie, M.F., and Fischer, F.R. (2015). Site-specific substitutional boron doping of semiconducting armchair graphene nanoribbons. J. Am. Chem. Soc. 137, 8872–8875.

17. Durr, R.A., Haberer, D., Lee, Y.L., Blackwell, R., Kalayjian, A.M., Marangoni, T., Ihm, J., Louie, S.G., and Fischer, F.R. (2018). Orbitally matched edge-doping in graphene nanoribbons. J. Am. Chem. Soc. 140, 807–813.

18. Rizzo, D.J., Veber, G., Cao, T., Bronner, C., Chen, T., Zhao, F., Rodriguez, H., Louie, S.G., Crommie, M.F., and Fischer, F.R. (2018). Topological band engineering of graphene nanoribbons. Nature 560, 204–208.

19. Gröning, O., Wang, S., Yao, X., Pignedoli, C.A., Borin Barin, G., Daniels, C., Cupo, A., Meunier, V., Feng, X., Narita, A., et al. (2018). Engineering of robust topological quantum phases in graphene nanoribbons. Nature 560, 209–213.

20. Narita, A., Feng, X., Hernandez, Y., Jensen, S.A., Bonn, M., Yang, H., Verzhbitskiy, I.A., Casiraghi, C., Hansen, M.R., Koch, A.H., et al. (2014). Synthesis of structurally well-defined and liquid-phase-processable graphene nanoribbons. Nat. Chem. 6, 126–132.

21. Narita, A., Verzhbitskiy, I.A., Frederickx, W., Mali, K.S., Jensen, S.A., Hansen, M.R., Bonn, M., De Feyter, S., Casiraghi, C., Feng, X., and Müllen, K. (2014). Bottom-up synthesis of liquid-phase-processable graphene nanoribbons with near-infrared absorption. ACS Nano 8, 11622–11630.

22. Joshi, D., Hauser, M., Veber, G., Berl, A., Xu, K., and Fischer, F.R. (2018). Super-resolution imaging of clickable graphene nanoribbons decorated with fluorescent dyes. J. Am. Chem. Soc. 140, 9574–9580.

23. Perkins, W., and Fischer, F.R. (2017). Inserting porphyrin quantum dots in bottom-up synthesized graphene nanoribbons. Chemistry 23, 17687–17691.

24. Matsumoto, M., Valentino, L., Stiehl, G.M., Balch, H.B., Corcos, A.R., Wang, F., Ralph, D.C., Mariñas, B.J., and Dichtel, W.R. (2018). Lewis-acid-catalyzed interfacial polymerization of covalent organic framework films. Chem 4, 308–317.

25. Sahabudeen, H., Qi, H., Glatz, B.A., Tranca, D., Dong, R., Hou, Y., Zhang, T., Kuttner, C., Lehnert, T., Seifert, G., et al. (2016). Wafer-sized multifunctional polyimine-based two-dimensional conjugated polymers with high mechanical stiffness. Nat. Commun. 7, 13461.

26. Dai, W., Shao, F., Szczerbiński, J., McCaffrey, R., Zenobi, R., Jin, Y., Schlüter, A.D., and Zhang, W. (2016). Synthesis of a two-dimensional covalent organic monolayer through dynamic imine chemistry at the air/water interface. Angew. Chem. Int. Ed. Engl. 55, 213–217.

27. Shekhirev, M., Vo, T.H., Pour, M.M., Lipatov, A., Munukutla, S., Lyding, J.W., and Sinitskii, A. (2017). Interfacial self-assembly of atomically precise graphene nanoribbons into uniform thin films for electronics applications. ACS Appl. Mater. Interfaces 9, 693–700.